Available online at www.sciencedirect.com
SCIENCE DIRECT
Polymer 46 (2005) 9928–9940
polymer
www.elsevier.com/locate/polymer

Vibrational and electronic properties of PPV-derived co-polymers: PPV–ether and C_{1-4}PPV–ether

A. Mabrouk[a], K. Alimi[a,*], M. Hamidi[b], M. Bouachrine[b], P. Molinié[c]

[a]*Laboratoire des Matériaux, Faculté des Sciences de Monastir, 5000 Monastir, Tunisia*
[b]*LRMM, Faculté des Sciences et Techniques, B.P. 509, Boutalamine, Errachidia, Morocco*
[c]*Institut des Matériaux Jean Rouxel, CNRS-UMR 6502, 2 Rue de la Houssinière, BP 32229, 44322 Nantes Cédex 3, France*

Received 2 November 2004; received in revised form 26 May 2005; accepted 19 July 2005
Available online 10 August 2005

Abstract

In this paper a combined experimental and quantum chemical study of two co-polymers, derived from poly(phenylene vinylene), referred to as PPV–ether and C_{1-4}PPV–ether, is presented. First, the geometries of these co-polymers were fully optimized. In fact, semiempirical, ab initio and density functional theory (DFT) have been used to investigate the ground-state properties of these co-polymers. Then, the electronic properties, lying in the excitation between the highest occupied molecular orbitals (HOMO) and the lowest unoccupied molecular orbitals (LUMO), the transition eigenvalues, the density of states together with other relevant physical quantities, were investigated. Moreover, the vibrational properties and the force constants are determined. In fact, the calculated results have well reproduced the available experimental data in which the pattern of dialkoxy-substitution is found to have a large effect.

Keywords: PPV derivative; Ab initio; DFT

1. Introduction

Most of recent papers are focused on the poly(phenylene vinylene) (PPV). Thanks to its important specific properties, this compound became the most promising materials for the optoelectronic device technology [1]. Based on results obtained from PPV, many other materials derived from this polymer are synthesized [2,3]. Within this scope, two new PPV derivative co-polymers denoted as PPV–ether (Scheme 1(a)) and C_{1-4}PPV–ether (Scheme 1(b)), have been synthesized. The interruption of conjugation in PPV motives by non-conjugated segments (ether motives) was meant to lead much higher quantum efficiency. Moreover, the introduction of alkoxy groups at specific positions was done in order to obtain materials with more predominant capability. PPV–ether and C_{1-4}PPV–ether, as it is the case of most polymers, are amorphous. And due to the absence of X-ray spectra and without reliable microanalyses it was not possible to infer their architecture experimentally. Indeed, the succession of the phenylene vinylene and ether motives can be either or by block or both. More details for their preparation and characterization have been largely described elsewhere [4,5]. In order to rationalize these experimentally observed properties of known materials and to predict those of unknown ones, theoretical investigations on the structures, electronic spectra and emissive properties of these materials are indispensable. In fact, it is well established that the semi empirical calculations can yield valuable information of PPV-derived co-polymers structures [6]. But, a full theoretical treatment including the effects of the strong electron–electron interactions, electron-lattice relaxation and inter-chain interactions, which are needed to fully describe PPV–ether co-polymer, is more suitable. For that matter, it is commonly believed that theoretical methods, especially those including electron correlation (ab initio and density functional theory (DFT)) are able to describe the geometry of organic molecules, as well as their energetics, in a satisfactory manner [7]. The present work is then, a combined experimental and quantum chemical study of geometrical vibrational and optoelectronic properties of PPV–ether and C_{1-4}PPV–ether. We perform a series of calculations on these co-polymers using

* Corresponding author. Tel.: +216 73 500 274; fax: +216 73 500 278.
E-mail address: kamel.alimi@fsm.rnu.tn (K. Alimi).

0032-3861/$ - see front matter © 2005 Elsevier Ltd. All rights reserved.
doi:10.1016/j.polymer.2005.07.060

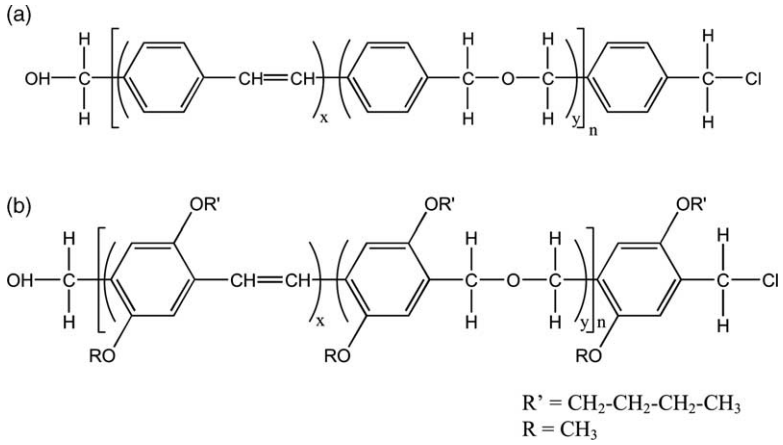

Scheme 1. The chemical structure of: (a) PPV–ether and (b) C_{1-4}PPV–ether.

semiempiric, ab initio, DFT and configuration interaction singles (CIS) methods. Our major goal is to understand and interpret the experimental absorption, emission spectra, and vibrational spectra. Then, to investigate the effect of alkoxy groups, attached on phenylene ring, on various properties of PPV–ether co-polymer.

2. Computations

The molecular quantum chemical calculations were performed at the semi-empirical, ab initio and DFT level. All the calculations have been carried out with Gaussian 98 program [8]. The computational procedure has been organized as follows: a first simulation is performed to equilibrate the system, where the structures are fully optimized by the quantum mechanical semi-empirical module. At our disposal: the Austin's Model (AM1) [9]. After that, and according to the large molecules model, all the calculations were done with a fast method based on the Hartree–Fock (HF) theory, which could only be carried out with smaller basis sets such as (3-21G(d)) [10]. In parallel, we have carried out a density functional theory (DFT) study using the most popular Becke's three-parameter hybrid functional, B3, with non-local correlation of Lee–Yang–Parr, LYP [11], abbreviated as B3LYP, method [12]. This method, based on DFT for a uniform electron gas (local spin density approximation), is used with the same basis set. In the 3-21G(d) basis set, d-orbitals have been added to non-hydrogen atoms such as carbon and oxygen atoms. In the case of the dialkoxy-substituted co-polymer and for the calculations, all the alkoxy substituents were taken to be methoxy groups. This simplification is not expected to significantly influence the results with regard to electronic effects of the substituents.

Furthermore, vibrational frequencies calculations have been carried out with HF/3-21G(d) method on fully geometry optimized structure and force constants were carried out using MOPAC 2000 program [13]. The ground state energies and oscillator strengths were then investigated using the configuration interaction singles (CIS/3-21G(d)) approach for PPV–ether and C_{1-4}PPV–ether on fully DFT optimized geometries. In fact, these calculations method have been successfully applied to poly(*para*-phenylene) (PPP) [14], PPV [15] and other conjugated polymers [16].

We have also examined HOMO (the highest occupied molecular orbital) and LUMO (the lowest unoccupied molecular orbital) levels, HOMO-LUMO gaps and vertical excitation energies (λ_{max}) [17] for the two materials under study.

3. Results and discussion

3.1. Geometric parameters

The PPV–ether co-polymer prepared in this research is sufficiently long to consider the translation as a symmetry operation. In the geometric structure of this co-polymer, and in order to be coherent with experimental results, three motives of PPV correspond to six other motives of ether in oligomer units. The geometric structure, displayed in Fig. 1 cannot exist in reality, but, due to the large molecule, this oligomer model allows us to investigate systems in the absence of disorder and limited length. This structure seems to be the better since the succession of PPV motives reflecting the experimental optical properties. The optimization process (the global minimum energy information of the materials is achieved) was fully done using three different methods (AM1, HF/3-21G(d) and B3LYP/3-21G(d)). The same calculation results are obtained also for the short length chain (Fig. 2) which will be used as a model for all other calculations. The internal coordinates set as main interatomic distance are labelled in Table 1. These data are in close agreement with those already obtained for PPV [18]. The other geometric characteristics set as angles and dihedral angles are collected in Tables 2 and 3. As it was shown in the previous study based on the experimental data

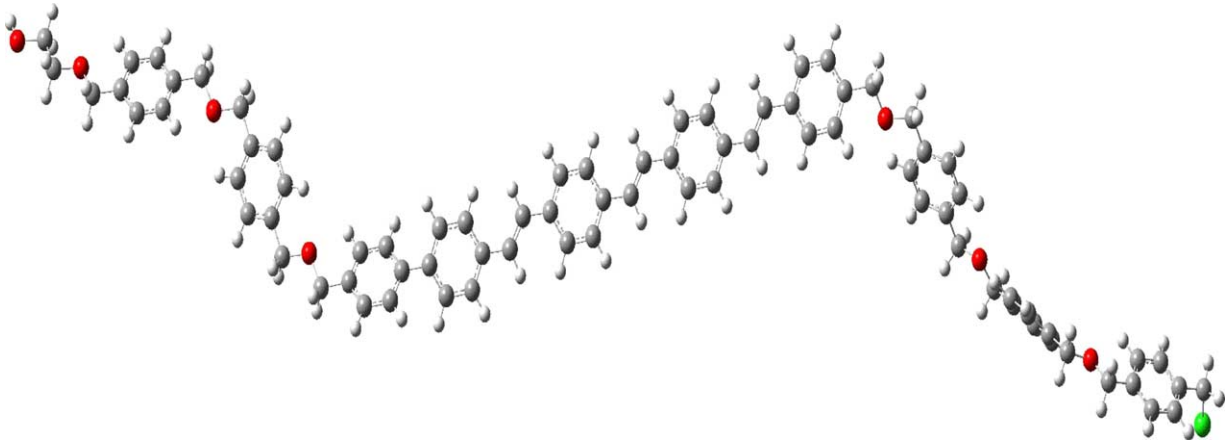

Fig. 1. The B3LYP/3-21G(d) optimized structure of PPV–ether.

supported by infrared absorption (IR) and resonance Raman scattering (RRS) measurements [19], we have proposed a geometrical structure for PPV–ether and C_{1-4}PPV–ether as compared to that of PPV but, the presence of ether groups, within the chain, induce certainly considerable modifications in geometric structures as in the case of PPV interrupted with silicon atoms [20]. Moreover, the optimized geometrical structure of the alkoxy-substituted PPV–ether was displayed in Fig. 3. On the resonance magnetic nuclear (NMR) ^{13}C solid state spectra of PPV–ether and C_{1-4}PPV–ether (Fig. 4), we have labelled the different carbon sites confirming the proposed structures. Added to those initially observed for PPV–ether, new peaks, which are located in the range of 0–50 ppm, were attributed to substitutent groups (methoxy and butoxy).

An accurate representation of the bond rotations in the chain is extremely important, since especially the properties of polymers depend strongly on the conformational statistics of the polymer chains. The theoretical calculations for the PPV–ether show a small coplanirity of the chain lattice having C_1 as a point group. The PPV moiety of the polymer chain is maintained planar. Only, the inter-ring torsion angle in ether motives part was evaluated to be about 40° as it in the case of PPP [21,22]. In fact, the torsion angle constitutes a compromise between the effect of conjugation and the steric repulsion between hydrogen, which favours a non-planar structure.

The effect of methoxy and butoxy groups grafted on 2 and 5 positions of phenyl ring is clearly seen. The ether motives are markedly affected with substitution of phenyl ring with alkoxy groups. Since, starting from the torsion angle, we notice that there is a considerable reduction of torsion angles in ether motives which is not the case in PPV motives. The steric effect of the chlorine atom with the alkoxy groups was found to be very small. When compared to HF and AM1 method, DFT yields longer C=C bonds and shorter C–C interring bonds, thus at DFT electron are more delocalized. This is most likely due to taking account of electron correlation. On the other hand, the substitution of alkoxy groups slightly lengthens some bonds and shortens

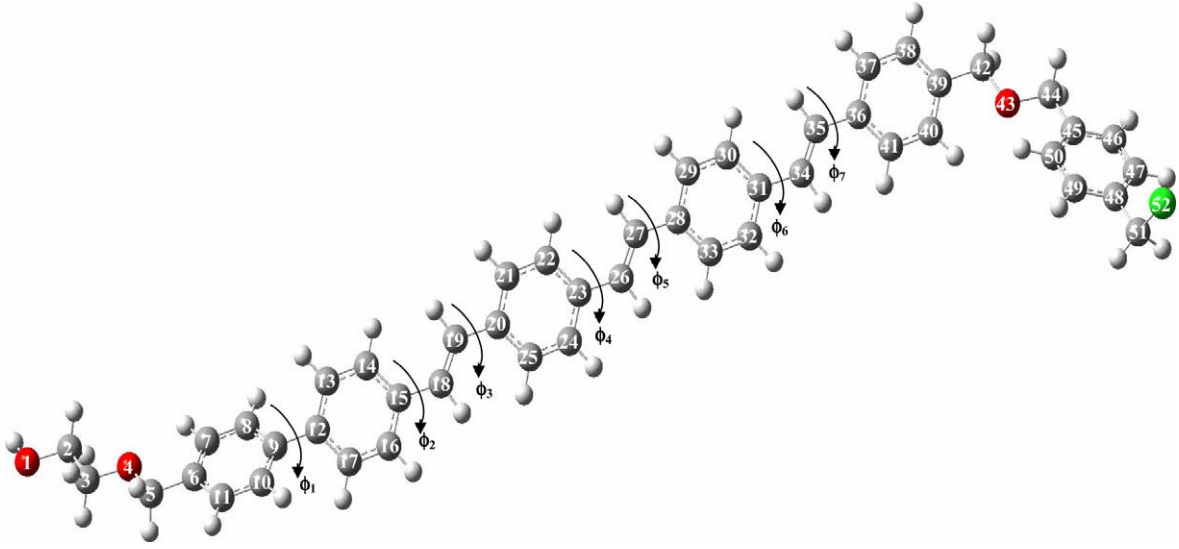

Fig. 2. The B3LYP/3-21G(d) optimized model structure of PPV–ether.

Table 1
Interatomic distance in optimized structure of PPV–ether and C_{1-4}PPV–ether

Bond (Å)	PPV–ether			C_{1-4}PPV–ether		
	AM1	HF/3-21G(d)	B3LYP/3-21G(d)	AM1	HF/3-21G(d)	B3LYP/3-21G(d)
C_5–C_6	1.492	1.513	1.517	1.490	1.506	1.508
C_7–C_8	1.393	1.383	1.393	1.395	1.374	1.388
C_9–C_{10}	1.403	1.391	1.406	1.411	1.390	1.416
C_{14}–C_{15}	1.402	1.391	1.410	1.398	1.387	1.403
C_{15}–C_{16}	1.404	1.391	1.409	1.416	1.393	1.412
C_{15}–C_{18}	1.452	1.475	1.456	1.451	1.470	1.586
C_{18}–C_{19}	1.343	1.325	1.348	1.344	1.326	1.350
C_{19}–C_{20}	1.452	1.475	1.463	1.451	1.47	1.457
C_{22}–C_{23}	1.402	1.391	1.410	1.399	1.389	1.405
C_{23}–C_{26}	1.452	1.475	1.462	1.451	1.469	1.456
C_{26}–C_{27}	1.343	1.325	1.349	1.344	1.326	1.351
C_{27}–C_{28}	1.452	1.475	1.462	1.451	1.470	1.457
C_{28}–C_{33}	1.402	1.391	1.410	1.399	1.388	1.405
C_{31}–C_{34}	1.452	1.475	1.464	1.451	1.470	1.581
C_{36}–C_{37}	1.405	1.391	1.409	1.416	1.471	1.417
C_{40}–C_{41}	1.393	1.381	1.389	1.398	1.380	1.391
C_{39}–C_{42}	1.492	1.512	1.514	1.493	1.506	1.506
C_{42}–O_{43}	1.428	1.434	1.457	1.432	1.447	1.476
O_{43}–C_{44}	1.428	1.433	1.455	1.419	1.436	1.461
C_{45}–C_{50}	1.397	1.382	1.397	1.391	1.373	1.387
C_{51}–Cl_{52}	1.761	1.830	1.858	1.762	1.833	1.867

other ones, as it mentioned in Table 1. This modification in bond length correlated with that of the corresponding angle, as quoted in Table 2, indicates an increment in the more conductive character in C_{1-4}PPV–ether. In fact, the conjugation across phenylene rings and vinylene motives is increased due to the stronger electron donating effect of alkoxy groups. The atomic charges were more sensitive to changes in conformation, especially during the C(sp2)–O(sp3) rotation. In the whole, the conformational changes in atomic charges between PPV–ether and C_{1-4}PPV–ether

Table 2
Angle in optimized structure of PPV–ether and C_{1-4}PPV–ether

Angle (°)	PPV–ether			C_{1-4}PPV–ether		
	AM1	HF/3-21G(d)	B3LYP/3-21G(d)	AM1	HF/3-21G(d)	B3LYP/3-21G(d)
C_3–O_4–C_5	111.6	115.7	113.0	109.2	115.4	112.8
O_4–C_5–C_6	109.0	109.0	108.5	109.2	108.7	108.3
C_{11}–C_6–C_7	119.4	119.1	119.2	118.7	119.3	119.3
C_6–C_7–C_8	120.2	120.2	120.3	120.8	119.9	119.8
C_9–C_{10}–C_{11}	120.4	120.5	120.7	120.9	120.0	121.0
C_{12}–C_{13}–C_{14}	120.5	120.9	121.2	121.0	119.9	120.2
C_{15}–C_{16}–C_{17}	120.6	121.1	121.4	121.0	120.2	120.3
C_{15}–C_{18}–C_{19}	124.5	125.5	126.8	124.5	125.9	126.2
C_{18}–C_{19}–C_{20}	124.5	125.5	126.7	124.5	125.8	126.1
C_{20}–C_{21}–C_{22}	120.7	121.2	121.6	121.1	120.2	120.3
C_{23}–C_{24}–C_{25}	120.7	121.2	121.6	121.1	120.2	120.3
C_{23}–C_{26}–C_{27}	124.7	125.6	126.7	124.6	125.9	126.2
C_{26}–C_{27}–C_{28}	124.7	125.5	126.7	124.5	125.8	126.1
C_{28}–C_{29}–C_{30}	120.7	121.2	121.6	121.1	120.2	120.3
C_{31}–C_{32}–C_{33}	120.7	121.2	121.6	121.1	120.2	120.3
C_{31}–C_{34}–C_{35}	124.5	125.5	126.7	124.6	125.8	126.0
C_{34}–C_{35}–C_{36}	124.5	125.5	126.7	124.5	125.5	126.1
C_{36}–C_{37}–C_{38}	120.5	120.9	121.2	120.9	120.0	120.0
C_{39}–C_{40}–C_{41}	120.2	120.3	120.5	120.8	119.7	119.6
C_{39}–C_{42}–O_{43}	109.0	108.8	108.2	107.5	107.1	106.5
C_{42}–O_{43}–C_{44}	111.6	115.6	112.9	113.2	115.8	112.5
O_{43}–C_{44}–C_{45}	108.9	108.7	108.2	114.1	111.3	111.5
C_{45}–C_{46}–C_{47}	120.2	120.4	120.2	120.8	119.5	119.2
C_{48}–C_{49}–C_{50}	120.3	120.7	120.6	120.7	119.4	119.2
C_{48}–C_{51}–Cl_{52}	111.7	111.3	111.3	111.9	111.4	111.5

Table 3
Dihedral angle in optimized structure of PPV–ether and C_{1-4}PPV–ether

Dihedral Angle (°)	PPV–ether			C_{1-4}PPV–ether		
	AM1	HF/3-21G(d)	B3LYP/3-21G(d)	AM1	HF/3-21G(d)	B3LYP/3-21G(d)
ϕ_1	39.8	49.1	40.0	44.8	44.5	35.5
ϕ_2	22.2	25.4	0.2	−20.8	3.3	−0.3
ϕ_3	−158.6	−155.2	−179.6	−158.9	176.0	179.6
ϕ_4	19.3	−24.3	−0.0	−18.8	−1.7	−1.0
ϕ_5	161.3	155.6	179.7	161.4	177.4	178.9
ϕ_6	−22.0	−25.4	−0.9	−19.1	−8.0	−2.2
ϕ_7	158.0	154.5	178.9	160.9	167.8	176.6

were less than 0.2 e. This can be evidence generally for the reduction of the dihedral angle. But in taking account, in the same time, for the steric effect, induced by the substitutent groups, a little increase for dihedral angle should take place as it discussed earlier.

3.2. Electronic properties

In Fig. 5, we report the normalised experimental absorption and emission energies of PPV–ether and C_{1-4}PPV–ether. Experimentally, the optical density (OD) was carried out, at room temperature, using a Carry 2300 spectrophotometer in the range of wavelengths from 0 to 3000 nm. concerning the photoluminescence (PL) measurements, the powder was placed in a conical hole under a SiO_2 window in the cryostat at 10 K, where the excitation of 1 mW was ensured by an argon laser. When examining the optical data, it is seen that the most striking feature, for the alkoxy substituted PPV–ether co-polymer, is the shift of the long wavelength absorption peak of PPV–ether resulting from the symmetry breaking of the aromatic ring. The experimental study shows that alkoxy substitution of the PPV–ether results in an absorption spectrum which is red-shifted with respect to 470 nm to be 512 nm. The emission spectrum which peaks at 610 nm shows a vibrational structure. In fact, the photoluminescence spectrum displays a hypsochromic shift for the C_{1-4}PPV–ether as compared to the unsubstiuted one with a corresponding longer natural radiative lifetime [23]. The red shifted emission to lower energy can be attributed to the formation of interchain dimer excitations as it was described earlier in the case of substituted PPV [24,25].

In Table 4, we present HOMO and LUMO energy, ΔE (the calculated energy differences between LUMO and HOMO), the absorption λ_{max} and oscillator strength as a result of all theoretical methods in comparison to those of experimental data, where the DFT method was the well reproduced one. The most relevant from this table is that the lateral substitution of phenyl ring with donor group (methoxy and butoxy) decreases the gap energy by approximatively 0.3 eV with decreasing the oscillator strength. A common way to judge the theoretical transition energies, calculated by CIS/3-21G(d) method, is to compare the calculations with the experimental absorption band as it

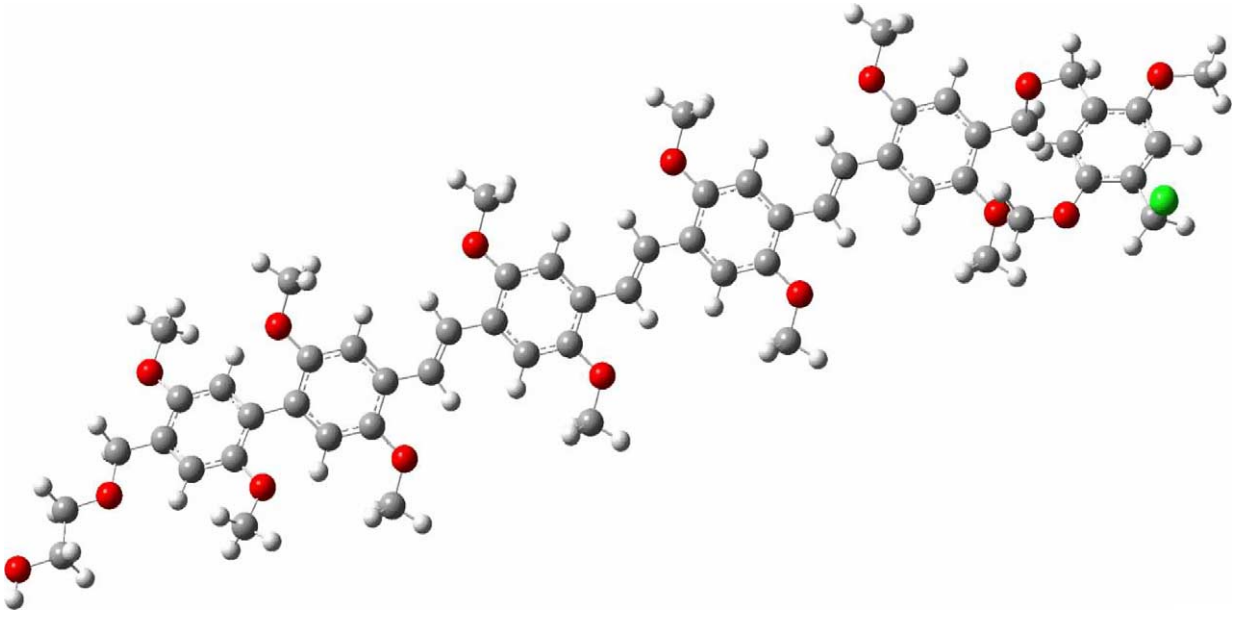

Fig. 3. The B3LYP/3-21G(d) optimized model structure of C_{1-4}PPV–ether.

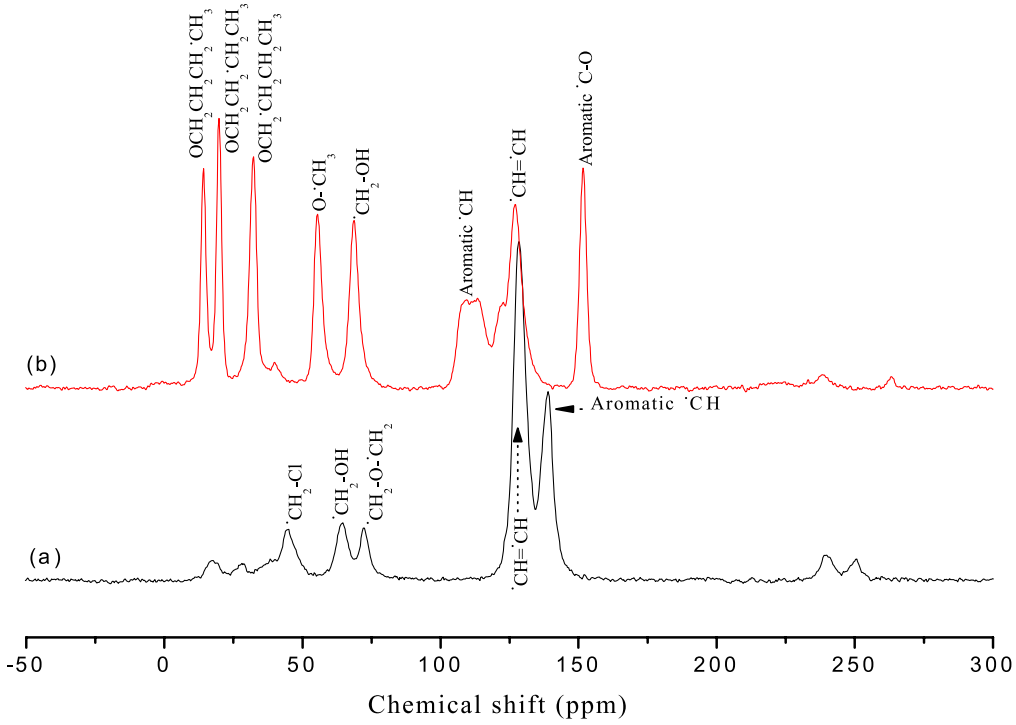

Fig. 4. ^{13}C NMR spectra of: (a) PPV–ether and (b) C_{1-4}PPV–ether.

was reported in Table 5 and shown in Fig. 6, where a good agreement was observed.

The theoretical calculations show clearly that HOMO-LUMO energy gap of PPV–ether was markedly reduced compared to that of PPV. The calculated excitation energies, which have high oscillator strength, are generally dominated by HOMO-LUMO transition [26]. As it can be seen, the dialkoxy-substituted PPV–ether shows a much smaller band gap than the unsubstituted one. In fact, this phenomena was already explained in the case of PPV [27] by the destabilization of the HOMO of the polymer chain through the antibonding interaction with the π-type orbital of the oxygen presented in the alkoxy group, since this electron donor group elevated the HOMO and LUMO level. Then, vertical excitation energies (λ_{max}) were calculated from extrapolated HOMO-LUMO gaps, as the same from band structure calculations employing Block orbitals, and compared to the corresponding λ_{max} in the observed

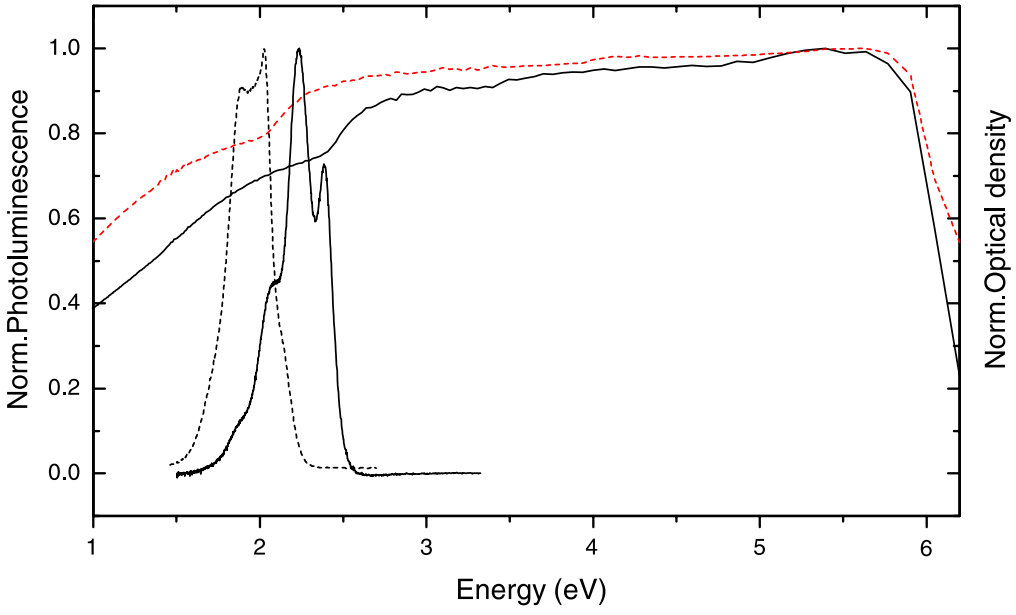

Fig. 5. Normalised optical density and PL spectra of: — PPV–ether and …. C_{1-4}PPV–ether.

Table 4
The optoelectronic parameters of PPV–ether and C_{1-4}PPV–ether

	PPV–ether						C_{1-4}PPV–ether					
	Calculated value					Experimental result	Calculated value					Experimental result
	HOMO	LUMO	ΔE	UV λ_{max}	O.S.	E_g UV λ_{max}	HOMO	LUMO	ΔE	UV λ_{max}	O.S.	E_g UV λ_{max}
AM1	−8.13	−0.87	7.26	239.46	4.4538	2.30 470	−7.71	−0.82	6.89	258.16	4.2037	2.01 512
HF/3-21G(d)	−7.15	−1.70	5.45	274.65	3.6630		−6.35	−1.63	4.72	315.96	3.5766	
B3LYP/3-21G(d)	−5.07	−1.98	3.09	437.24	3.2078		−4.35	−1.69	2.66	514.38	2.8329	

Calculated HOMO (eV), LUMO (eV), ΔE (=LUMO-HOMO) (eV), absorption λ_{max} (nm), oscillator strength (O.S.), as well as experimental gap E_g (eV) and absorption λ_{max} (nm) for PPV–ether and C_{1-4}PPV–ether.

absorption spectra of co-polymer. This approach was parameterized to reproduce band gaps defined as the λ_{max} for the π–π^* transition of conjugated polymers, and not the band edges which are often used to define the gaps experimentally. In fact, the band gap obtained with DFT method is in close agreement with the extrapolated band gap from experimental absorption spectra (Fig. 6). In fact, the density functional calculation method, which account for electron correlation, yielded much more accurate values for the HOMO-LUMO gap than the Hartree–Fock method.

Generally, we argued that the theoretical band gaps calculated for isolated chains are expected to be about 0.2 eV larger than the condensed phase values [28]. However, it is believed that the bulk or intermolecular effects must be taken into account when considering the polymers with long chains [29]. After correcting this effect, our theoretical band gaps agree well with experiment.

In order to gain greater insight into the difference between the pristine and the substituted PPV–ether, it is worthwhile to plot their highest occupied (HOMO) and lowest unoccupied (LUMO) molecular orbital. In our case, the HOMO is an antibonding vinylene orbital and the π orbital of the central phenyl ring whereas the LUMO is a bonding combination of an anti-bonding vinylene orbital and a π^* orbital of phenyl ring. As for as these geometries, the energy diagram of PPV–ether and C_{1-4}PPV–ether co-polymers are shown in Figs. 7 and 8, respectively. Just like PPV–ether, the HOMO→LUMO transition of the dialkoxy substituted PPV–ether is delocalized over the whole PPV motives but within a next extended part over the dialkoxy groups.

The HOMO→LUMO transition in PPV–ether occurs with an oscillator strength of 3.207 (Table 5), this elevated value indicates an important photoabsorption degree. The second excited state has a very small oscillator strength of 0.005, which is a 1000-fold decrease in magnitude. In C_{1-4}PPV–ether, The HOMO→LUMO transition occurs with an oxillator strength of 2.832 which become 0.007 in the third state transition with three contributing orbitals.

3.3. Vibrational study

The main purpose of vibrational studies is to assign Raman and Infrared modes to characterize the electronic structure of these co-polymers. For that, we consider the full DFT-optimized geometry which allows us to distinguish between in-plane and out-of-plane vibrations. The vibrational assignments of the FTIR and RRS spectra of the pristine co-polymer have been previously reported [19]. Experimentally, Infrared spectra were obtained in a Bruker Vector 22 spectrophotometer where the samples were pellets of KBr mixed with the organic compounds under study. Moreover, the Raman spectra were recorded on a Fourier transform spectrometer Bruker RFS 1000 with 1064 nm-wavelength laser.

In order to confirm the proposed assignment, theoretical vibrational calculations were performed. The experimental

Table 5
Calculated and experimental transition energies (ΔE), calculated oscillator strengths and main CI expansion coefficient of PPV–ether and C_{1-4}PPV–ether

Compound	Transition	ΔE Exp. (eV)	ΔE Calc. (eV)	f (Calc.)	Main CI-expansion coefficients
PPV–ether	T_1	2.85	2.83	3.207	0.65 (H→L)
	T_2	3.35	3.34	0.005	0.56 (H−1→L)−0.42 (H→L+1)
	T_3	3.70	3.69	0.001	0.36 (H−1→L)+0.5 (H→L+1)
C_{1-4}PPV–ether	T_1	2.40	2.41	2.832	0.64 (H→L)
	T_2	2.81	2.86	0.127	0.61 (H−1→L)−0.3 (H→L+1)
	T_3	3.10	3.11	0.007	0.4 (H−2→L)+0.2 (H−1→L)+0.47 (H→L+1)

and theoretical frequencies and their assignments are presented in Tables 6 and 7 where all peaks are identified. The theoretical Infrared and Raman spectra of the PPV–ether and C_{1-4}PPV–ether are displayed in Figs. 9 and 10, respectively. Generally, the characteristics of the vibrations of individual entities contribute to several modes whose frequencies are close to each other.

In the Infrared spectra of PPV–ether, we can distinguish the main vibration modes characteristics of the proposed structure. In low frequency, the in plane quadrant ring bend is localized at 543 cm^{-1}. A very weak band appears at 669 cm^{-1} which is assigned to C–C aromatic out of plane bending. The band at 854 cm^{-1} corresponds to C–Cl terminal group stretching. Moreover, the weak C–H aromatic out of plane bending and aliphatic C–H rocking are located at 902 cm^{-1}. The band at 1255 cm^{-1} is for aliphatic C–H rocking of terminal group and aromatic C–C stretching at 1325 cm^{-1}. We can also notice that the aliphatic C–H rocking and wagging are located, respectively, at 1468 and 1431 cm^{-1}. Besides, the antisymmetric $-CH_2$ stretching is observed at 3032 cm^{-1}. These bands are in close agreement with those reported in the paper of Bradely [30].

In the Infrared spectra of C_{1-4}PPV–ether, we note the bands already described for PPV–ether and new bands characteristics of dialkoxy substituted ring. The shoulder which appears at 1307 cm^{-1} is related to the in-plane $O-CH_3$ deformation. The other observed differences are firstly, the shortness of the wide band at 796 cm^{-1} related to in-plane aromatic C–C deformation and the antisymmetric

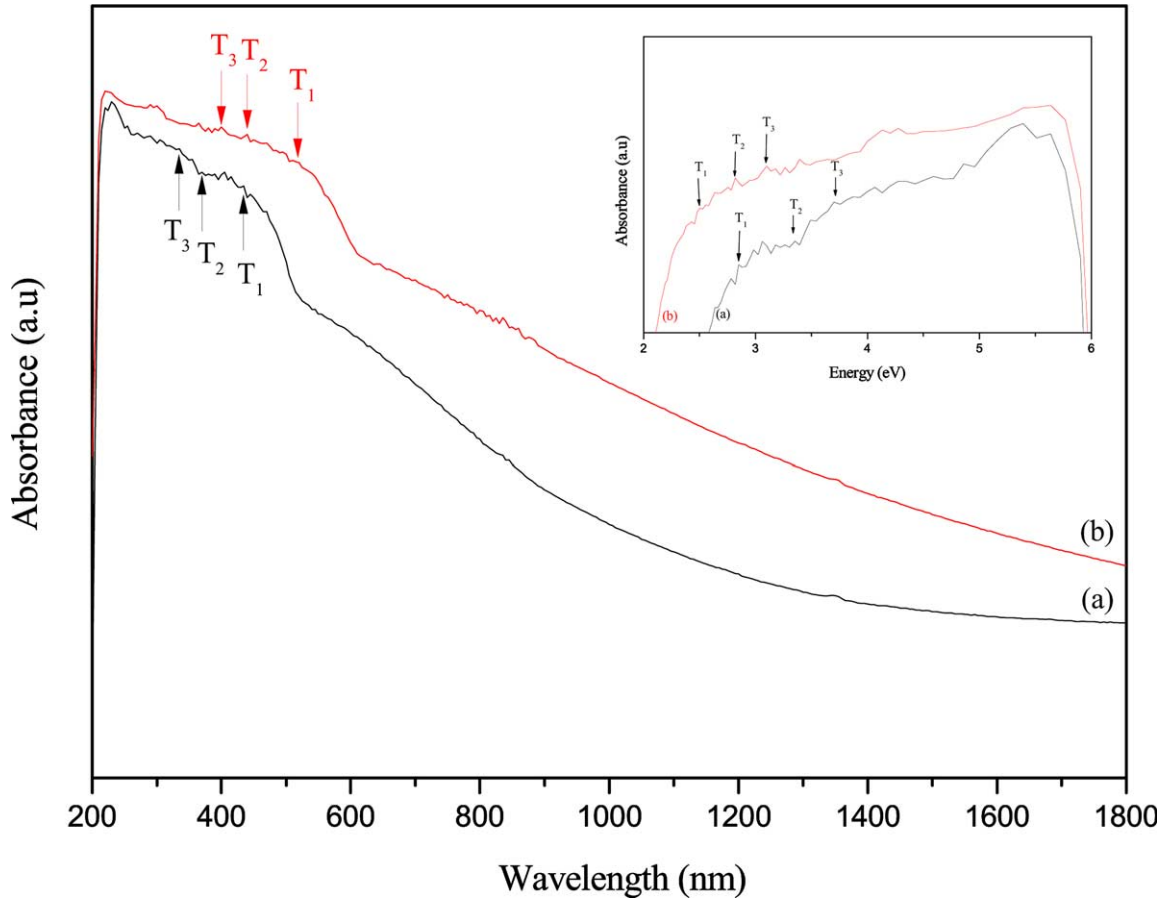

Fig. 6. Representation of experimental transitions.

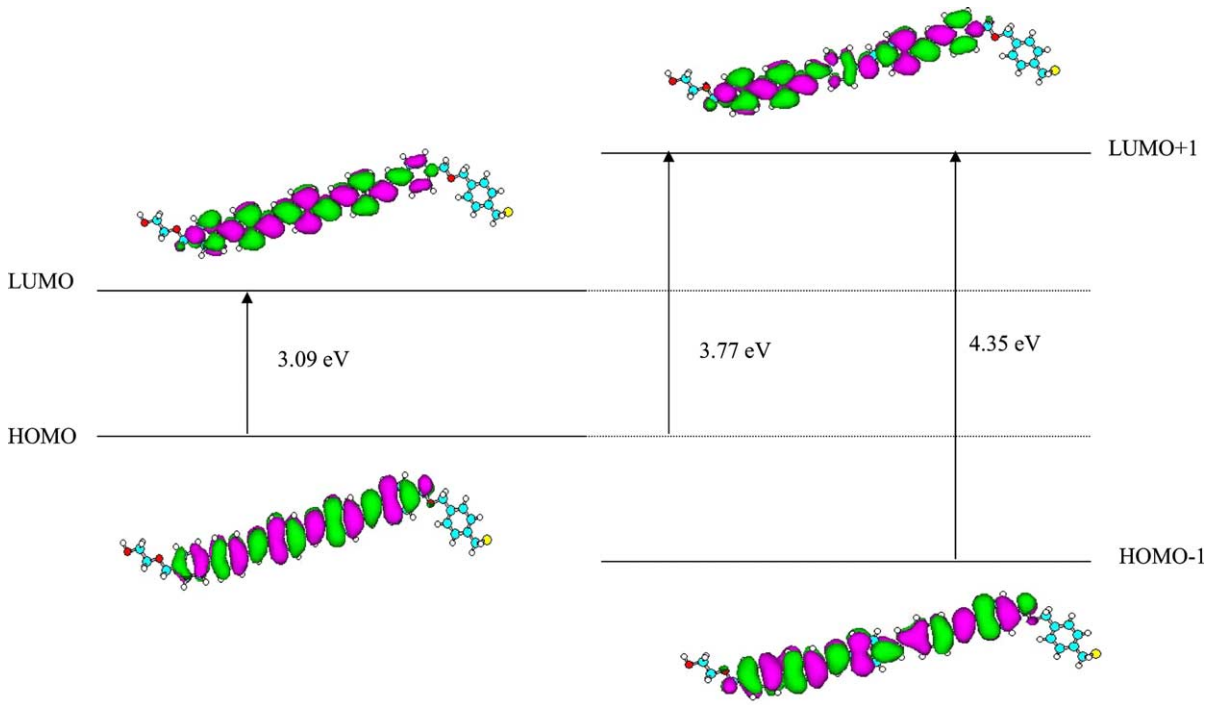

Fig. 7. Schematic representation of molecular orbitals and transitions for PPV–ether.

C–H vinylene out of plane bending located at 973 cm^{-1} and the strongest band related to aliphatic and aromatic C–H in plane wagging located at 1403 cm^{-1}. As far as ether vibration is concerned, the antisymmetric stretching located at 1374 cm^{-1} in PPV–ether disappeared and another one with strong intensity took place, in C_{1-4}PPV–ether, at 1370 cm^{-1} assigned to symmetric stretching. We also note the disappearance of the peak located at 1541 cm^{-1} associated to C–C aromatic stretching. The other difference lies in the appearance of strong peaks in the range of about

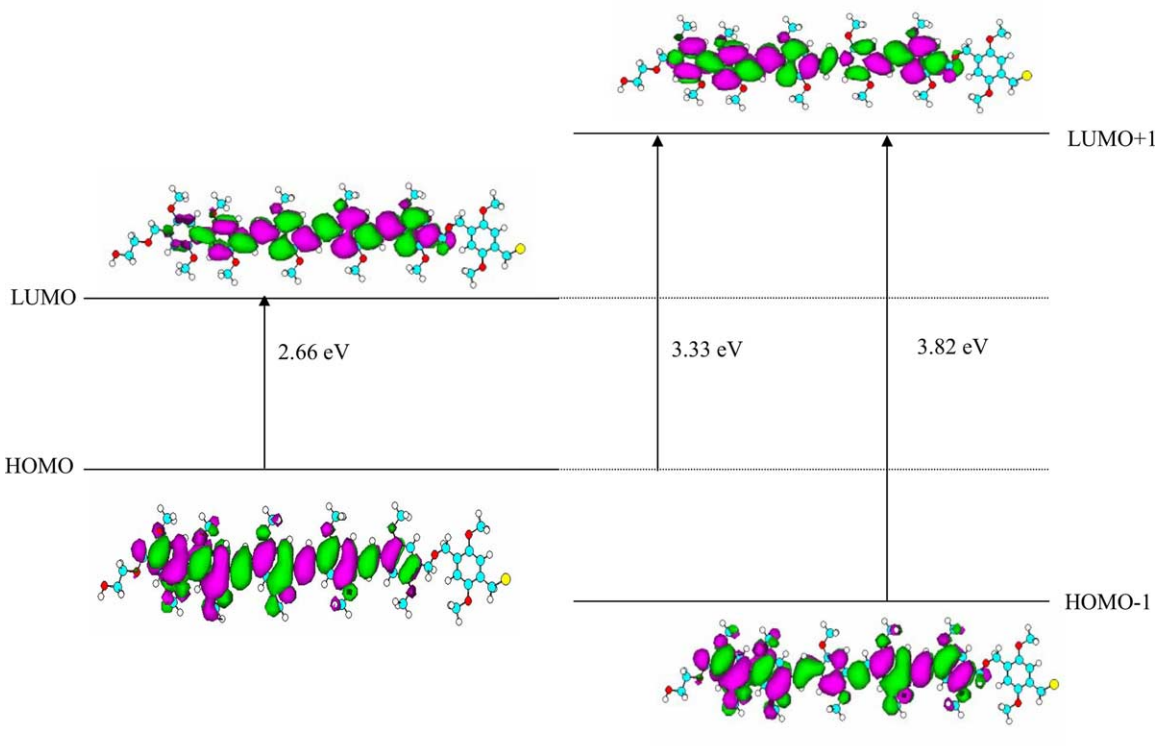

Fig. 8. Schematic representation of molecular orbitals and transitions for C_{1-4}PPV–ether.

Table 6
Experimental and calculated wavenumbers ($\bar{\nu}$) of infrared bands for PPV–ether and C_{1-4}PPV–ether

PPV–ether				C_{1-4}PPV–ether				Assignments
Exp. Freq. (cm^{-1})	I	Cal. Freq. (cm^{-1})	I	Exp. Freq. (cm^{-1})	I	Cal. Freq. (cm^{-1})	I	
542	w	543	vw	477	vw	549	Vw	In-plane quadrant ring bend
–	–	577	w	598	–	–	–	Quadrant bend out of plane ring
629	w	–	–	–	–	–	–	Aromatic out of plane quadrant bend
686	w	669	vw	678	m	709	Vw	Aromatic C–C out of plane bending
761	vw	796	s	736	w	740	Vw	In plane Aromatic C–C bending
828	m	854	m	860	m	837	M	C–Cl terminal group stretching
920	vw	902	vw	–		918	w	Aromatic out of plane C–H bending + aliphatic C–H rocking
961	m	973	s	965	m	981	m	Antisymmetric C–H vinylene out of plane bending
1020	m	–	–	1032	s	–	–	Aromatic C–H in plane bending + aliphatic C–C stretching
1079	m	–	–	1066	m	1070	vw	In plane aromatic and aliphatic C–H bending
1168	vw	–	–	1202	vs	1176	vw	Aliphatic C–H out of plane rocking
1270	vw	1255	m	1231	vw	1256	w	Aliphatic C–H rocking of terminal group
–	–	–	–	–	–	1307	m	$–O–CH_3$ stretching
1355	w	1325	w	1345	m	1358	m	Aromatic C–C stretching
–	–	–	–	–	–	1370	s	Symmetric $–CH_2–O–CH_2–$ stretching
–	–	1374	m	–	–	–	–	Antisymmetric $–CH_2–O–CH_2–$ stretching + in plane C–H rocking
1418	m	1403	w	1400	w	1417	vs	Aliphatic and aromatic C–H in plane wagging
–	–	1431	m	1409	s	1438	m	Aliphatic C–H wagging
–	–	1468	m	1462	s	1481	w	Aliphatic $–CH_2$ rocking
1510	m	1541	w	1501	s	–	–	Aromatic C–C stretching
1579	vw	1565	w	1600	m	1591	vw	Symmetric C–C aromatic stretch
1606	w	1647	w	1640	w	1646	v	Symmetric C–C aromatic stretch
–	–	–	–	–	–	1659	vs	Antisymmetric quadrant ring stretch
1695	m	–	–	–	–	1675	s	Antisymmetric quadrant ring stretch (terminal group)
–	–	–	–	–	–	1701	w	Antisymmetric in plane C=C aromatic stretch
–	–	1668	w	1800	vw	1803	vw	In plane C=C aromatic stretch
–	–	1696	m	–	–	–	–	C–C inter-ring stretching
1900	w	–	–	2110	vw	–	–	C=C vinylene stretching
2844	vw	–	–	2864	m	–	–	Aliphatic $–CH_2$ rocking
2923	vw	3032	vw	2927	m	3032	vw	Antisymmetric $–CH_2$ stretching
3022	w	3159	vw	3053	w	3089	vw	Symmetric $–CH_2$ stretching
–	–	3175	s	–	–	3166	m	Antisymmetric aromatic C–H stretch (terminal group)
–	–	3186	vs	–	–	3190	m	Aromatic C–H stretch (terminal group)
3326	vw	3502	m	–	–	3500	m	OH stretch (chain ends)

vs: very strong; s: strong; m: mean; w: weak and vw: very weak.

1659 and 1675 cm^{-1} could correspond, respectively, to antisymmetric quadrant ring stretch within the chain lattice and in terminal groups. The latter localised at 1701 cm^{-1} is attributed to antisymmetric ring stretch. Other peaks are mainly reduced to disappear at 1696 and 1900 cm^{-1} where C–C inter-ring stretch and C=C vinylene stretching became inactive as the alkoxy groups attached to the phenyl ring have just prohibited these vibrations. In high frequency range, a great similarity was observed except that the intensity of aromatic C–H stretching of terminal groups is considerably decreased.

The main results derived from this refined Raman calculations show that, in the two cases, the strong Raman intensities are especially caused by C=C and C–C of phenyl ring stretching accompanied by C=C vinylene stretching detected, respectively, at around 1551, 1590 and 1634 cm^{-1}. These vibrations become stronger in the case of alkoxy substituted PPV–ether showing a more conjugated character in a well defined structure. As it can be noticed from Fig. 10, although, the small shift of theoretical spectra to higher wavenubers, the main difference between the spectra of the two co-polymers is the appearance of two new peaks; the first was located at 1281 cm^{-1} attributed to in plane C–H vinylene wagging and antisymmetric C–C aromatic stretch whereas, the second peak associated to aromatic C=C stretch appear towards 1447 cm^{-1}. In addition, to confirm the proposed assignment for infrared spectra of PPV–ether, theoretical vibrational calculations were performed. A least squares fitting procedure with minimising standard deviation X was applied in order to adjust the calculated wavenumbers to the experimentally recorded values.

Table 7
Experimental and calculated wavenumbers ($\bar{\nu}$) of Raman bands for PPV–ether and C_{1-4}PPV–ether

PPV–ether				C_{1-4}PPV–ether		Assignments
Exp. Freq. (cm^{-1})	I	Cal. Freq. (cm^{-1})	I	Exp. Freq. (cm^{-1})	I	
–	–	–	–	601	w	C–C stretching of phenyl ring
963	vw	753	vw	963	w	C–H *trans*–vinylene out of plane bending
–	–	–	–	1111	m	In plane C–C stretch
1172	M	1086	m	1175	vw	Aromatic C–H in plane bending
–	–	–	–	1281	s	In plane C–H vinylene wagging + antisymmetric aromatic C–C stretch
1325	vw	1213	vw	1312	s	Aromatic C–C stretching
1416	vw	1279	w	1407	vw	Aromatic and vinylene C–H bending
–	–	–	–	1447	vw	Aromatic C=C stretching
1551	w	1581	M	1550	vw	C=C stretching of the phenyl ring
1590	s	1630	S	1586	vs	Aromatic C–C stretching
1634	w	1711	M	1626	w	Vinylene C=C stretching

vs: very strong; s: strong; m: mean; w: weak and vw: very weak.

$$X = \left[\frac{1}{N}\sum_{i=1}^{N}\left(w^{i}_{\mathrm{exp}} - w^{i}_{\mathrm{calc}}\right)^{2}\right]^{1/2}$$

Where w^{i}_{exp} and w^{i}_{calc} are the observed and the calculated wavenumbers of the vibration i, respectively, and N is the number of observed wavenumbers. The X value is found to be 31 cm^{-1} for PPV–ether and 40 cm^{-1} for C_{1-4}PPV–ether. The set of in-plane force constants resulting from the optimization process is given in Table 8. With the internal coordinates already discussed, we defined in-plane vibrations of the two copolymers.

The force constants are defined by:

$$F_{RR'} = \left[\frac{\partial^{2}\Phi}{\partial R \partial R'}\right]_{0}$$

where Φ is the potential energy, R and R' are two internal coordinates.

The parameters which reflect the electronic structure of the backbones are especially those corresponding to the PPV motives. The semiempirical relationship between carbon–carbon bond length and the corresponding stretching force constants is defined as:

$$F_{\mathrm{C-C}}\alpha(1/r^{4}_{\mathrm{CC}})$$

In fact, all chemical and structural changes occurring upon grafting alkoxy substitutent on aromatic ring of PPV–ether

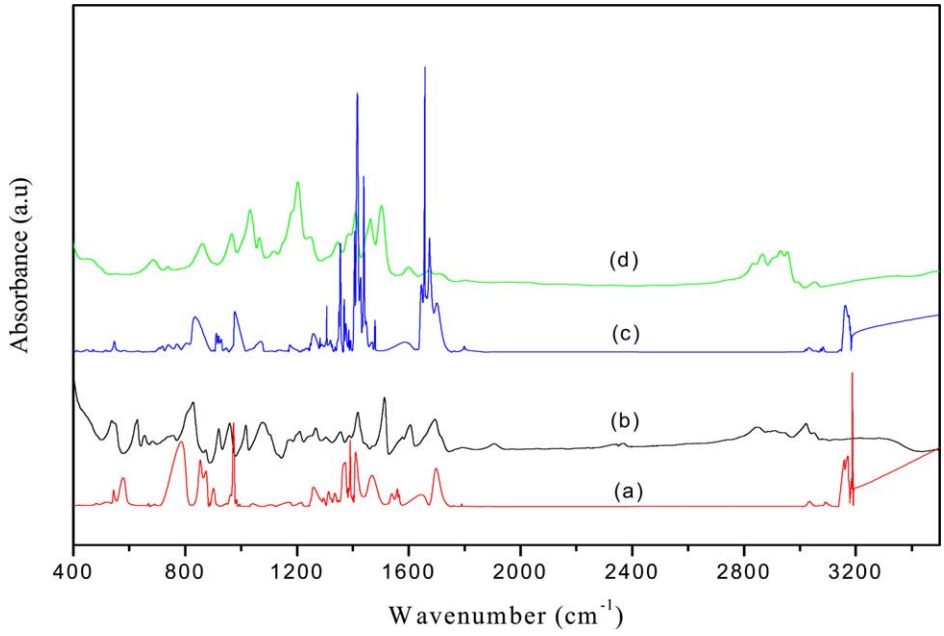

Fig. 9. Infrared: (a) theoretical spectra of PPV–ether, (b) experimental spectra of PPV–ether; (c) theoretical spectra of C_{1-4}PPV–ether and (d) experimental spectra of C_{1-4}PPV–ether.

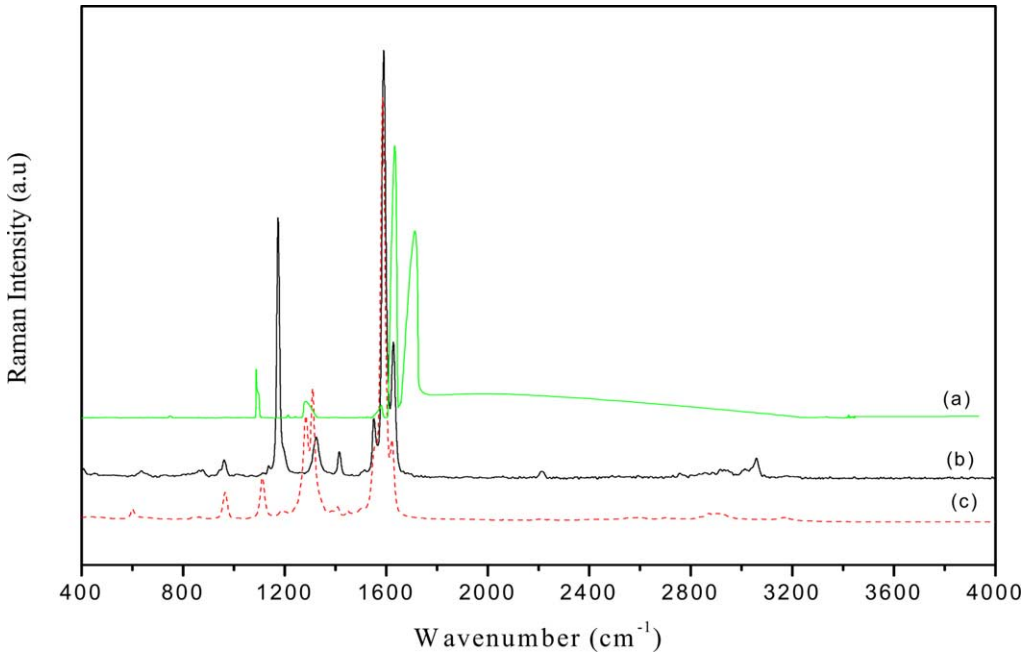

Fig. 10. Raman: (a) theoretical spectra of PPV–ether; (b) experimental spectra of PPV–ether and (b) experimental spectra C_{1-4}PPV–ether.

should give rise to significant modification of force constant. We note firstly, that the optimized values reflect the different bond orders where the force constants relating to aromatic ring correspond to an average between those of carbon inter-ring and the carbon of vinyl groups. Moreover, it should be pointed out that the alkoxy substuting results in a little decrease of C=C vinyl (C_{18}–C_{19}, C_{26}–C_{27} and C_{34}–C_{35}) force constant accompanied by an increase of the force

Table 8
Force constant (Millidyne/Angôstrom) of PPV–ether and C_{1-4}PPV–ether

PPV–ether		C_{1-4}PPV–ether	
$F_{O1-C2}=5.28$	$F_{C27-C28}=5.41$	$F_{O1-C2}=5.25$	$F_{C27-C28}=5.53$
$F_{C2-C3}=4.59$	$F_{C28-C29}=5.89$	$F_{C2-C3}=4.58$	$F_{C28-C29}=5.61$
$F_{C3-O4}=4.97$	$F_{C29-C30}=6.66$	$F_{C3-O4}=5.05$	$F_{C29-C30}=6.48$
$F_{C4-C5}=5.10$	$F_{C30-C31}=6.00$	$F_{C4-C5}=5.03$	$F_{C30-C31}=6.09$
$F_{C5-C6}=4.59$	$F_{C31-C32}=5.90$	$F_{C5-C6}=4.80$	$F_{C31-C32}=5.65$
$F_{C6-C7}=6.41$	$F_{C32-C33}=6.66$	$F_{C6-C7}=6.26$	$F_{C32-C33}=6.47$
$F_{C7-C8}=6.45$	$F_{C33-C28}=6.00$	$F_{C7-C8}=6.46$	$F_{C33-C28}=6.09$
$F_{C8-C9}=6.14$	$F_{C31-C34}=5.39$	$F_{C8-C9}=6.01$	$F_{C31-C34}=5.52$
$F_{C9-C10}=6.08$	$F_{C34-C35}=9.17$	$F_{C9-C10}=5.73$	$F_{C34-C35}=9.07$
$F_{C10-C11}=6.52$	$F_{C35-C36}=5.33$	$F_{C10-C11}=6.19$	$F_{C35-C36}=5.44$
$F_{C11-C6}=6.30$	$F_{C36-C37}=6.00$	$F_{C11-C6}=6.71$	$F_{C36-C37}=5.67$
$F_{C9-C12}=5.09$	$F_{C37-C38}=6.52$	$F_{C9-C12}=4.95$	$F_{C37-C38}=6.35$
$F_{C12-C13}=6.02$	$F_{C38-C39}=6.36$	$F_{C12-C13}=5.64$	$F_{C38-C39}=6.44$
$F_{C13-C14}=6.61$	$F_{C39-C40}=6.28$	$F_{C13-C14}=6.42$	$F_{C39-C40}=6.12$
$F_{C14-C15}=6.00$	$F_{C40-C41}=6.57$	$F_{C14-C15}=6.15$	$F_{C40-C41}=6.40$
$F_{C15-C16}=5.99$	$F_{C41-C36}=6.01$	$F_{C15-C16}=5.82$	$F_{C41-C36}=6.13$
$F_{C16-C17}=6.54$	$F_{C39-C42}=4.56$	$F_{C16-C17}=6.39$	$F_{C39-C42}=4.80$
$F_{C17-C12}=6.14$	$F_{C42-O43}=4.91$	$F_{C17-C12}=6.12$	$F_{C42-O43}=4.32$
$F_{C15-C18}=5.36$	$F_{O43-C44}=4.96$	$F_{C15-C18}=5.51$	$F_{O43-C44}=4.71$
$F_{C18-C19}=9.14$	$F_{C44-C45}=4.64$	$F_{C18-C19}=9.03$	$F_{C44-C45}=4.54$
$F_{C19-C20}=5.39$	$F_{C45-C46}=6.31$	$F_{C19-C20}=5.51$	$F_{C45-C46}=6.17$
$F_{C20-C21}=5.90$	$F_{C46-C47}=6.50$	$F_{C20-C21}=5.62$	$F_{C46-C47}=6.39$
$F_{C21-C22}=6.66$	$F_{C47-C48}=6.25$	$F_{C21-C22}=6.48$	$F_{C47-C48}=6.25$
$F_{C22-C23}=6.00$	$F_{C48-C49}=6.28$	$F_{C22-C23}=6.07$	$F_{C48-C49}=6.05$
$F_{C23-C24}=5.89$	$F_{C49-C50}=6.46$	$F_{C23-C24}=5.63$	$F_{C49-C50}=6.22$
$F_{C24-C25}=6.66$	$F_{C50-C45}=6.37$	$F_{C24-C25}=6.47$	$F_{C50-C45}=6.66$
$F_{C25-C20}=6.00$	$F_{C48-C51}=3.38$	$F_{C25-C20}=6.09$	$F_{C48-C51}=4.52$
$F_{C23-C26}=5.41$	$F_{C51-Cl52}=2.46$	$F_{C23-C26}=5.54$	$F_{C51-Cl52}=2.29$
$F_{C26-C27}=9.10$		$F_{C26-C27}=8.98$	

constant related to C–C interring (C_{15}–C_{18}, C_{19}–C_{20}, C_{23}–C_{26}, C_{27}–C_{28}, C_{31}–C_{34} and C_{35}–C_{36}). In addition, the substituted ring is characterized by an important decrease of C=C force constant (with butoxy and methoxy group substituted carbon; e.g.: C_{12}–C_{13}, C_{13}–C_{14}, C_{15}–C_{16}, C_{16}–C_{17}). And the others remain fairly unchanged. The above results are very consistent with experimental data and the already modifications observed in Raman and infrared spectra of the two compounds with taking into account experimental conditions.

4. Conclusion

We set up a theoretical model where our calculations suggest a good correspondence between the excitation energies and the optical properties, obtained by CIS/3-21G(d), calculated in the present work and the experimental data. In fact, this study suggests that the geometric optimized structures obtained by the DFT method are more accurate than those obtained by using AM1 and HF. The DFT can, thus, be reliably used in single chain property calculations and in studies on bulk material properties containing structural units studied in this work. The introduction of alkoxy substituents (butoxy and methoxy groups) on phenylene ring was found to have a large effect on the PPV–ether co-polymer properties. In addition to the modification in geometric parameters, the substitution of electron donating on the phenyl ring destabilized the HOMO and LUMO levels with decreasing the oxillator strength where the degree of delocalisation were obtained from the DFT charge distribution and a red shift was observed in the absorption and emission spectrum of the substituted co-polymer. The analysis of vibrational features and the derived force constant argue very well for the proposed structures showing the effect of substituted alkoxy groups. This study has been shown to yield remarkably reliable band structures for a wide variety of conjugated polymers, including those with heteroatoms.

This approach can be used to study fruitfully the perturbations induced by doping along the polymeric chains. Further theoretical investigations are necessary in order to advance our understanding of the interface phenomena in polymer LEDs.

Acknowledgements

This work has been supported by Tunisio–Marocain cooperation (02/TM/16).

References

[1] Nguyen T-P, Molinié P, Destruel P. In: Nalwa HS, editor. Handbook of advanced electronic and photonic materials and devices. Light-emitting diodes, lithuim batteries and polymer devices, vol. 10. New York: Academic press; 2001.
[2] Friend RH, Gymer RW, Holmes AB, Burroghes JH, Marks RN, Taliani C, et al. Nature (London) 1999;397:121.
[3] Pusching P, Ambrosch DC. Phys Rev B 1999;60(11):7891–8.
[4] Alimi K, Molinié P, Blel N, Fave JL, Bernede JC, Ghedira M. Synth Met 2002;126:19–25.
[5] Alimi K, Molinié P, Majdoub M, Bernede JC, Fave JL, Bouchriha H, et al. Eur Polym J 2001;37:781–7.
[6] Park Y, So Y, Chung S-J, Jin J-I. J Korean Phys Soc 2000;37(1): 59–63.
[7] Grozema FC, Candeias LP, Swart M, Van Duijnen PTh, Wildemen J, Hadziioanou G, et al. J Chem Phys 2002;117(24):11366–78.
[8] Frisch MJ, Trucks GW, Schlegel HB, Scuseria GE, Rubb MA, Cheeseman JR, Zakrzewski VG, Montgomery JA, Stratmann RE, Burant JC, Dapprich S, Millam JM, Daniels AD, Kudin KN, Strain MC, Farkas O, Tomasi J, Barone V, Cossi M, Cammi R, Mennucci B, Pomelli C, Adamo C, Clifford S, Ochterski J, Petersson GA, Ayala PY, Cui Q, Morokuma K, Malick DK, Rabuck AD, Raghavachari K, Foresman JB, Cioslowki J, Ortiz JV, Stefanov BB, Liu G, Liashenko A, Piskorz P, Komaromi I, Gomperts R, Martin RL, Fox DJ, Keith T, Al-Laham MA, Peng CY, Nanayakkara A, Gonzalez C, Challacombe M, Gill PMW, Johnson BG, Chen W, Wong MW, L Andres J, Head-Gordon M, Replogle ES, Pople JA. GAUSSIAN 98, Gaussian Inc.: Pittsburgh, PA; 1998.
[9] Dewar HJS, Zoebisch EG, Healy EF, Steward JJP. J Am Chem Soc 1985;107:3902.
[10] Pietro WJ, Francl MM, Hehre WJ, Defrees DJ, Pople JA, Binkley JS. J Am Chem Soc 1982;104:5039.
[11] Lee C, Yang W, Parr RG. Phys Rev B 1988;37:785.
[12] Becke AD. J Chem Phys 1996;104:1040.
[13] Stewart JJP. Fujitsu Limited, Tokyo, Japan; 1999.
[14] Förner W. J Mol Struct (Theochem) 2004;682:115–36.
[15] Wang B-C, Chang J-C, Pan J-H, Xue C, Luo F-T. J Mol Struct (Theochem) 2003;636:81–7.
[16] Rabias I, Howlin BJ. Comput Theor Polym-Sci 2001;11:241–9.
[17] Zhou X, Ren A-M, Feng J-K. Polymer 2004;45:7747–57.
[18] Stalmach Ulf, Schollmeyer D, Meier H. Chem Mater 1999;11: 2103–6.
[19] Mabrouk A, Ayachi S, Zaidi B, Buisson JP, Molinié P, Alimi K. Eur Polym J 2003;39:2121–7.
[20] Seong S, Lee ME, Lee TB, No KT, Kim HK. Synth Met 2004;141: 251–7.
[21] Breads JL, Thémans B, Fripiat JG, André JM, Chance RR. Phys Rev B 1984;29(12):6761–72.
[22] Grein F. J Mol Struct (Theochem) 2003;624:23–8.
[23] Pogantsch A, Mahler AK, Hayn G, Saf R, Stelzer F, List EJW, et al. J Chem Phys 2004;297:143–51.
[24] Pu Y-J, Kurata T, Soma M, Kido J, Nishide H. Synth Met 2004;143: 207–14.
[25] Pinto MR, Hu B, Karasz FE, Akcelrud L. Polymer 2000;41:2603–11.
[26] Hong SY. Bull Korean Chem Soc 1999;20(1):42–8.
[27] Lagowski JB. J Mol Struct (Theochem) 2002;589–590:125–37.
[28] Salzner U, Lagowski JB, Pickup PG, Poirier RA. Synth Met 1998;96: 177–89.
[29] Lagowski JB. J Mol Struct (Theochem) 2003;634:243–52.
[30] Bradely DDC. J Phys D Appl Phys 1978;20:1389–410.